

Early-stage memory effect on the dephasing charger-mediated quantum battery

Yu Wang and Jiasen Jin*

School of Physics, Dalian University of Technology, 116024 Dalian, China

(Dated: February 17, 2026)

We investigate the performance of the charger-mediated quantum battery modeled by a two-qubit system. One of the qubits acts as the battery and the other acts as the charger which is subjected to a reservoir. We derived the time-local master equation in Lindblad form with a time-dependent dephasing rate. The dephasing rate may be negative in the early-stage of the charging process and thus indicate the presence of the memory effect. We find that such early-stage memory effect could increase the maximal ergotropy of the battery compared with the one under Markovian approximation with the corresponding asymptotic dephase rate. The enhancement of the performance is explained by means of the non-Markovian quantum jumps. Moreover, a discrete time scheme of the measurement-enhanced quantum battery is proposed in a quantum circuit with global and random local operations.

I. INTRODUCTION

The quantum effects, including the quantum coherence and entanglement, become more and more pronounced in the micro- and nano scale systems [1]. This has spurred the development of quantum devices which exhibit exotic properties and superior performance compared to their classical counterparts. Among the quantum devices, the quantum battery, as a device for temporarily storing and transferring energy, has attracted significant attention in the past years [2]. The simplest model of a quantum battery in discrete-variable systems is the two-level system. A large variety of intriguing implementations of quantum battery with the charging and discharging process under the unitary dynamics have been reported in the single and many-body systems [3–21].

The inevitable interaction between the quantum systems and its surrounding environments always leads to the loss of coherence, thus generally entails the degradation of the performance of a quantum battery [22]. In contrast, the dissipation can also be viewed as a resource to boost the charging of quantum battery with a mediated system named as the charger [23]. Usually the dynamics of the charger and quantum battery can be described by the so-called Markovian process during which the information of the system flows to the environment. Indeed, the Markovian approximation is valid, at least for capturing the behavior of the long-time evolution when the time resolution is much larger than the time scale over which the environment correlation decays.

However, the non-Markovian dynamics is ubiquitous in practical quantum systems [24, 25]. The non-Markovianity can be used to enhance the performance of quantum batteries [26, 27]. A typical example is the time-evolution of a qubit interacting with a structured environment which can be described by a Markovian master equation over a large time scale of evolution [28, 29]. The non-Markovianity featured by the information backflow, although lasts shortly, is visible in the early stage of the evolution. For quantum batteries, more attention is paid to their charging capability in short time, therefore it is interesting to investigate how the early-

stage non-Markovianity affects the dynamics of a quantum battery. It would also be benefit for a more accurate assessment of quantum battery performance in the presence of the dissipation.

In this work, we shed light on the impact of the early-stage non-Markovianity on the performance of a charger-mediated quantum battery (CmB) which is modeled by two interacting qubits. One of the qubits acts as the battery and the other acts as the charger which is subjected to a reservoir with the Lorentzian density spectrum. Through a microscopic derivation we obtain the time-local master equation in Lindblad form that describes the dynamics of the CmB system [30, 31]. A powerful tool to simulate the dynamics governed by such master equation is the quantum jump method, which considers the stochastic time-evolution of a large number of pure states [32–35]. In the standard quantum jump method, the state of each realization evolves either continuously governed by an effective non-Hermitian Hamiltonian or undergoes normal quantum jumps during the period of positive decay rate.

In the secular region of the considered CmB system, the time-dependent decay rate can be temporarily negative which features the non-Markovianity of the dynamics. In Refs. [36, 37], the negative decay rate is interpreted as the possibility for the system to recover the state before decoherence. The revival of the coherence is realized by the action of the reversed quantum jump that cancels the previous normal quantum jump in the period of positive decay rate. However, when the non-Markovian quantum jump (NMQJ) method is extended to the many-body or driven systems, it is rather challenge due to the dramatically increased trajectory number.

Considerable efforts has been devoted in generalizing the NMQJ method [38–43]. The diagrammatic method developed by Chiriacó *et al.* allows to analytically calculate the probability of the trajectories in the NMQJ framework [44]. Inspired by this technique, one of the authors has simplified the formalism for the driven-dissipative qubit system [45] which is naturally suited for the CmB system presented in Sec. II. By combining the Runge-Kutta (RK) method and the NMQJ method, we provide the evidence that the early-stage memory effect may increase the maximal ergotropy at the end of the charging process of the CmB. We also propose a discrete-time scheme for enhancing the performance of the CmB with random local operation in the early-stage evolution.

*Electronic address: jsjin@dlut.edu.cn

The paper is organized as follows. In Sec. II we demonstrate the model of the CmB system and present the time-local master equation in the Schrödinger picture. To simulate the non-Markovian dynamics with negative dephasing rate, we introduce the non-Markovian quantum jump method in Sec. IV. In Sec. III, we investigate the influence of the early-stage memory effects on the performance of the quantum battery. A measurement-enhanced quantum battery is proposed in Sec. V. We summarize in Sec. VI.

II. THE MODEL

We consider a CmB system consisting of two qubits with one acting as the charger, denoted by A , and the other acting as the quantum battery, denoted by B . The charger is subjected to a thermal bosonic reservoir denoted by E , as shown in Fig. 1(a). The free Hamiltonians of the subsystems A , B and E are given as follows (set $\hbar = 1$ hereinafter),

$$\hat{H}_A = \frac{\omega_A}{2} \hat{\sigma}_A^z, \quad (1)$$

$$\hat{H}_B = \frac{\omega_B}{2} \hat{\sigma}_B^z, \quad (2)$$

and

$$\hat{H}_E = \sum_k \omega_k \hat{a}_k^\dagger \hat{a}_k, \quad (3)$$

where $\hat{\sigma}_X^\alpha$ ($\alpha = x, y, z$ and $X = A, B$) represents the Pauli matrices acting on the subsystem X and \hat{a}_k is the annihilation operator of the k -th harmonic oscillator mode of the reservoir. The frequencies ω_A , ω_B and ω_k represents the energy separations of the charger, the battery and the energy of the k -th bosonic mode, respectively. In addition, the charger is driven by an external field as the energy supply via the following Hamiltonian,

$$\hat{H}_A^{\text{dr}} = \frac{\Omega}{2} (\hat{\sigma}_A^+ e^{-i\omega_L t} + \text{h.c.}), \quad (4)$$

where $\hat{\sigma}^\pm = (\hat{\sigma}^x \pm i\hat{\sigma}^y)/2$ are the corresponding raising and lowering operators. The ω_L and Ω is the frequency and the amplitude of the external driving field. Here we denote the detuning of the frequencies between the driving field and the charger as $\Delta = |\omega_A - \omega_L|$.

The Hamiltonians describing the charger-battery and the charger-reservoir interactions are given as follows,

$$\hat{H}_{AB} = g(\hat{\sigma}_A^+ \hat{\sigma}_B^- + \text{h.c.}), \quad (5)$$

$$\hat{H}_{AE} = \sum_k (g_k \hat{\sigma}_A^+ \hat{a}_k + \text{h.c.}), \quad (6)$$

where g and g_k are the coupling strength of charger with the battery, and with the k -th bosonic mode, respectively. In the limit of a continuum of the reservoir modes one has

$\sum_k |g_k|^2 \rightarrow \int d\omega J(\omega)$ where $J(\omega)$ is the spectral density function. In this work we focus on the reservoir with a Lorentzian spectral density,

$$J_{\text{Lor}}(\omega) = \frac{\eta^2}{2\pi} \frac{\lambda^2}{(\omega - \omega_0)^2 + \lambda^2}, \quad (7)$$

where ω_0 is the central frequency, λ is the width of the spectrum and η^2 denotes the effective coupling constant.

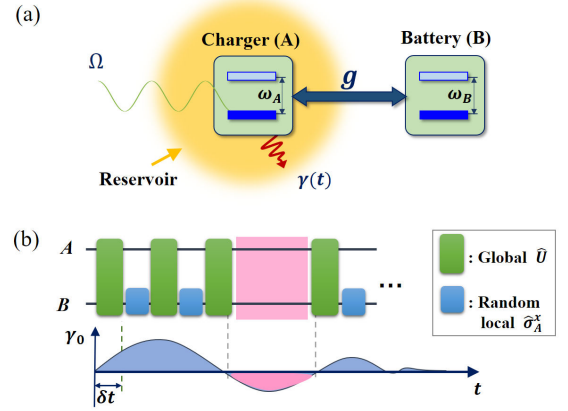


FIG. 1: (a) The model. The charger qubit is subjected to the reservoir while the battery qubit is isolated. The spectral densities of the reservoirs in both models are Lorentzian. The charger is driven by an external field as the energy supplier and interacts with the battery. (b) The quantum circuit diagram for the measurement-enhanced quantum battery. The global unitary operations \hat{U} acting on the charger (A) and the battery (B), alternate with the random local operations $\hat{\sigma}_A^x$ acting on the charger (A), in the $\gamma_0 > 0$ period of the early stage. The local operation is suspended on during the $\gamma_0 < 0$ period (red shaded region).

In the limit of weak coupling, one can obtain the time-local master equation describing the time-evolution of the joint state of the charger and the battery as follows,

$$\dot{\rho}_{AB}(t) = -i[\hat{H}_0 + \hat{H}_1, \rho_{AB}(t)] + \mathcal{D}[\rho_{AB}(t)], \quad (8)$$

where $\hat{H}_0 = -\frac{\Omega}{2} \hat{\sigma}_A^x + \frac{\omega_B}{2} \hat{\sigma}_B^z$ and $\hat{H}_1 = g(e^{i\omega_L t} \hat{\sigma}_A^+ \hat{\sigma}_B^- + \text{h.c.})$. As detailed in the Appendix, Eq. (8) is derived in the rotating frame with $e^{-i\omega_L \hat{\sigma}_A^x t/2}$ and under the resonant condition, i.e. $\omega_A = \omega_B = \omega_L$. The first term of the r.h.s. of Eq. (8) describes the unitary dynamics governed by $\hat{H}_0 + \hat{H}_1$. While the second term is the dissipator describing the dissipation induced by the reservoir and, in general, containing the secular and nonsecular terms [29]. Because the quantum battery is isolated from the reservoir, the dissipator acts locally on the charger.

In order to specify the dissipator \mathcal{D} in Eq. (8), two parameters are introduced as follows,

$$p = \frac{\tau_C}{\tau_A} = \frac{\sqrt{\Delta^2 + \Omega^2}}{\lambda}, \quad (9)$$

$$s = \frac{\omega_0 - \omega_L}{\lambda}, \quad (10)$$

where $\tau_C = \lambda^{-1}$ characterizes the time scale of the reservoir correlation and $\tau_A = (\Delta^2 + \Omega^2)^{-1/2}$ characterizes the typical time of the charger over which its state varies appreciably. The former parameter p identifies the region in which the secular approximation is valid, while the latter parameter s characterizes the detuning of the central frequency of the Lorentzian spectrum from the frequency of the driving field in units of λ .

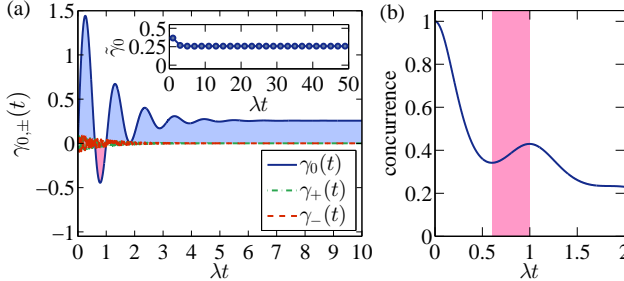


FIG. 2: (a) The time-dependence of the decay rates of the charger. The solid line denotes the behavior of γ_0 . In the early-stage $\lambda t \lesssim 4$, the positive γ_0 is punctuated by a segment with negative γ_0 . For $\lambda t \gtrsim 4$, the γ_0 remains positive and reach to the asymptotic value at large λt . The decay rates $\gamma_+(t)$ and $\gamma_-(t)$ oscillates between the positive and negative values. The amplitude is so small ($< 10^{-2}$) compared with γ_0 that can be neglected. The inset shows the coarse-grained value of γ_0 . The parameters are chosen as $p = 100$ and $s = 6$. (b) The concurrence of the CmB system with $g = 0$. The initial state is the maximally entangled state. A revival of entanglement can be observed during the period of negative γ_0 indicating the back flow of information. The shaded regions in red indicate the period of negative γ_0 .

Since the goal of this work is to highlight the non-Markovian effects on the performance of the CmB, we will focus on the case of $p \gg 1$ for which τ_A is much shorter than τ_C so that the nonsecular components in \mathcal{D} can be neglected [29, 37]. Moreover, if the typical frequency of the charger ω_A is far detuned from the central frequency of the reservoir ω_0 , i.e. $q \gg 1$, the decay rates for the incoherent loss and gain (denoted by γ_{\pm}) in the dissipator are suppressed. Therefore the dissipator \mathcal{D} is reduced to the following

$$\mathcal{D}[\rho_{AB}] = \gamma_0(t)(\hat{\sigma}_A^x \rho_{AB} \hat{\sigma}_A^x - \rho_{AB}), \quad (11)$$

where the time-dependent decay rate is given by

$$\gamma_0(t) = \frac{\eta^2(1 - e^{-\lambda t}[\cos(s\lambda t) - s \sin(s\lambda t)])}{4(1 + s^2)}. \quad (12)$$

In Fig. 2(a) it is shown the decay rates in the secular region with $p = 100$ and $s = 6$. One can see that (i) the amplitudes of the γ_{\pm} is much smaller than γ_0 indicating that the loss and gain processes are strongly suppressed; (ii) the γ_0 oscillates at the early stage and then asymptotically approaches to a positive constant $\gamma_0(\infty)$; and (iii) the γ_0 can be temporally negative during an intermediate period $0.6 \lesssim \lambda t \lesssim 1$. The positive decay rate indicates that the time-evolution of the composite system of the charger and the quantum battery is Markovian. On the contrary, the negative decay rate violates the complete

positive and trace-preserving of the quantum master and may give rise to the possibility for the system to recover the state before decoherence.

When the scale of the time resolution is large, the decay rate can be coarse-grained as $\tilde{\gamma}_0(T) = \frac{1}{T} \int_{t-T/2}^{t+T/2} \gamma_0(t) dt$ where T is the coarsening size. As shown in the inset of Fig. 2, the coarse-grained decay rate $\tilde{\gamma}_0$ with $T = \lambda t$ smooths out the non-Markovianity in the early-stage and the dynamics can be regarded as a Markovian process. Indeed the coarse-graining treatment is a good approximation for the case that the typical time scale of the system of interest is larger than T , or for investigating the steady-state property. However, when focusing on the temporal behavior in the early stage, such as the charging process of a quantum battery which is aimed to be completed in a period as short as possible, the details of $\gamma_0(t)$ should be taken into account. We will concentrate on the impact of the early-stage behavior of γ_0 in the next section.

III. PERFORMANCE OF THE QUANTUM BATTERY

Let us start by showing the memory effect during the period of negative decay rate by simulating the non-Markovian dynamics described by Eq. (8). We perform a direct integration of the master equation by using the standard forth-order RK method with the CmB system initialized in the maximally entangled state $|\psi\rangle_{AB} = \frac{1}{\sqrt{2}}(|\uparrow_A^z \downarrow_B^z\rangle + |\downarrow_A^z \uparrow_B^z\rangle)$, where $|\uparrow_X^{\alpha}\rangle$ and $|\downarrow_X^{\alpha}\rangle$ are the eigenvectors of $\hat{\sigma}_X^{\alpha}$ with the eigenvalues +1 and -1, respectively. The entanglement is measured by the concurrence [46]. For a two-qubit system in state ρ , the concurrence is given by $C(\rho) = \max\{0, \sqrt{\lambda_1} - \sqrt{\lambda_2} - \sqrt{\lambda_3} - \sqrt{\lambda_4}\}$ with $\lambda_1 \geq \lambda_2 \geq \lambda_3 \geq \lambda_4$ being the eigenvalues of the matrix $\rho(\hat{\sigma}^y \otimes \hat{\sigma}^y)\rho^*(\hat{\sigma}^y \otimes \hat{\sigma}^y)$.

Since the dissipator acts locally on the charger, the entanglement is expected to decrease monotonically in the Markovian dynamics. The time-evolution of the entanglement is shown in Fig. 2(b). A revival of entanglement can be observed in the period of $\gamma_0 < 0$ signaling the backflow of information from the reservoir to the system which is a feature of the non-Markovianity.

Now we investigate the performance of the CmB system with dephasing. We will focus on the charging process for an empty battery in the empty state $|\downarrow_B^z\rangle$. At the end of the charging process, the energy contained in the battery is given as follows,

$$E_B(t) = \frac{1}{2} \text{tr}[(\hat{\sigma}_B^z + \hat{\mathbb{I}}_B)\rho_{AB}(t)], \quad (13)$$

where $\hat{\mathbb{I}}_B$ is the identity matrix. Another figure of merit of the quantum battery is the ergotropy which quantifies the maximal extractable work under a cyclic unitary transformation U ,

$$\mathcal{E}_B(t) = E_B(t) - \min_{U \in \mathcal{U}_c} \{\text{tr}[\hat{H}_B \hat{U}_B \rho_B(t) \hat{U}_B^\dagger]\}, \quad (14)$$

where $\rho_B(t)$ is the reduced density matrix of the battery and \mathcal{U}_c is the set of cyclic unitary operations [47, 48]. For a qubit

battery with the free Hamiltonian (2), the mean-energy and the ergotropy can be obtained explicitly as follows,

$$E_B(\tau) = \frac{\omega_B}{2}[1 + r_z(\tau)], \quad (15)$$

$$\mathcal{E}_B(\tau) = \frac{\omega_B}{2}[r(\tau) + r_z(\tau)], \quad (16)$$

where $r(\tau)$ and $r_z(\tau)$ are the modulus and the z component of the Bloch vector associated with the $\rho_B(\tau)$ [23].

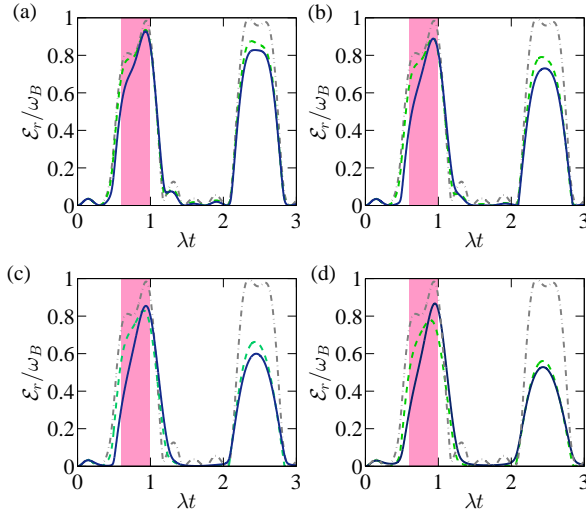


FIG. 3: The time-evolution of the ergotropy of the charger-mediated battery with $\omega_A = \omega_B = \omega_L = 100\lambda$, $\Omega = 0.1\omega_A$ and $g = 4$. The coupling strength between the charger and the reservoir in Eq. (12) are $\eta^2 = 0.5, 1, 2$ and 3 for panels (a)-(d). The initial state is $|\psi_{AB}(0)\rangle = |\uparrow_A^y \downarrow_B^z\rangle$. The solid, dashed, and dash-dotted lines represents the cases (i), (ii), and (iii), respectively. The shaded region in red indicates the period of $\gamma_0 < 0$.

For a concrete example, we specialize the parameters in Eqs. (1)-(5) as $\omega_A = \omega_B = \omega_L = 100\lambda$ and $\Omega = 0.1\omega_A$. The chosen parameters satisfy both the resonant condition and the requirement of secular approximation, and thus produce the decay rate $\gamma_0(t)$ in Fig. 2(a). In order to uncover the early-stage memory effect on the performance of the quantum battery, we investigate dynamics for three cases: (i) the non-Markovian dephasing with time-dependent decay in Eq. (12), (ii) the Markovian dephasing with a constant decay rate which is the asymptotic value of Eq. (12), i.e. $\gamma_0(\infty)$, and (iii) the unitary evolution without dephasing.

The dynamics of the ergotropy for various coupling strength between the charger and the reservoir are shown in Fig. 3. The behavior of the ergotropy under unitary time evolution shows the battery is maximally charged for the first time at $\lambda t \approx 0.95$, referred to as the charging time. The charging time in case (iii) is determined by the coupling strength g in Eq. (5) and could serve as a benchmark for cases (i) and (ii).

From Figs. 3(a) to 3(d), one can see that the peak of the ergotropy in cases (i) and (ii) is lowered due to the dephasing, and the height of the peak decreases as η increases. To be

specific, the charging time in case (ii) is shorten as the η increases but at a cost of the decreasing of the maximum of the ergotropy. Comparing the case (i) and (ii), the charging time in case (ii) is slightly shorter than that in case (i). More interestingly, the maximal ergotropy in case (i) becomes larger than that of case (ii) as the η increases. This can be understood as the following. In case (i), before the period of $\gamma_0 < 0$, the temporal magnitude $|\gamma_0(t)|$ oscillates around $\gamma_0(\infty)$ resulting in a stronger decoherence and thus a lower ergotropy compared to case (ii). While during the period of $\gamma_0(t) < 0$ (the shaded region in the panels), the information, previously lost into the reservoir, flows back to the CmB system to recover the behavior of case (iii) manifested by a rapid growth in (the steep slope of) the ergotropy. On the other hand, the large magnitude of the negative γ_0 indicates a strong memory effect, by means of more likely to implement the reversed quantum jump as will be seen soon, therefore the maximal ergotropy is close to that of case (iii) and higher than that of case (ii).

IV. NON-MARKOVIAN QUANTUM JUMP

The memory effect during the period of negative $\gamma_0(t)$ can be understood in the unraveling of the time-local master equation (8) with the NMQJ method. In the quantum jump method, Eq. (8) can be recast as follows,

$$\dot{\rho}_{AB}(t) = -i[\hat{H}_{\text{eff}}\rho_{AB}(t) - \rho_{AB}(t)\hat{H}_{\text{eff}}^\dagger] + \gamma_0(t)\hat{\sigma}_A^x\rho_{AB}(t)\hat{\sigma}_A^x, \quad (17)$$

where the non-Hermitian effective Hamiltonian is $\hat{H}_{\text{eff}} = \hat{H}_0 + \hat{H}_1 - i\gamma_0(t)\hat{I}/2$. An initial pure state evolves either continuously under the non-unitary operator $\exp(-i\hat{H}_{\text{eff}}t)$ or undergoes a discontinuous operation via the action of $\hat{\sigma}_A^x$. The density matrix in Eq. (8) can thus be represented as the following incoherent mixture of all the possible states of the members in the resulting ensemble,

$$\rho(t) = \sum_n K_n^\alpha(t) |\psi_n^\alpha(t)\rangle\langle\psi_n^\alpha(t)|, \quad (18)$$

where $|\psi_n^\alpha(t)\rangle$ denotes one of the possible states at time t and $K_n^\alpha(t)$ is the corresponding weight.

In the NMQJ method, the time axis is discretized by the time interval δt . In Ref. [45], different states $|\psi_n^\alpha\rangle$ are considered to originate from different quantum trajectories which are labeled by H_n^α with $\alpha = [t_1, t_2, \dots, t_w]$ being the time sequence that records the time at which the system undergoes a quantum jump and $n = \# \alpha$ being the number of quantum jumps. Here the quantum state refers to the CmB system and the subscript ‘AB’ has been omitted. Such *trajectory* describes the continuous time evolution of the system’s state governed by the effective non-Hermitian Hamiltonian starting from the time point $t = \alpha(n)$. Specially, the quantum state associated to the no-jump trajectory H_0^α at time t_s is given by

$$|\psi_0^\alpha(t_s)\rangle = \frac{\exp(-i\hat{H}_{\text{eff}}t_s)|\psi(t_0)\rangle}{\|\exp(-i\hat{H}_{\text{eff}}t_s)|\psi(t_0)\rangle\|}, \quad (19)$$

and the quantum state associated to a generic quantum trajectory H_n^α , with $\alpha = [\alpha', t_w]$, at $t_s > t_w$ is given by the following

recurrence relation

$$|\psi_n^\alpha(t_s)\rangle = \frac{\exp[-i\hat{H}_{\text{eff}}(t_s - t_w)]|\psi_n^\alpha(t_w)\rangle}{\|\exp[-i\hat{H}_{\text{eff}}(t_s - t_w)]|\psi_n^\alpha(t_w)\rangle\|}, \quad (20)$$

where $|\psi_n^\alpha(t_w)\rangle = \hat{\sigma}_A^x |\psi_{n-1}^{\alpha'}(t_w)\rangle / \|\hat{\sigma}_A^x |\psi_{n-1}^{\alpha'}(t_w)\rangle\|$.

To incorporate the memory effect during the period of $\gamma_0 < 0$, the set of trajectories H_n^α characterized by the time sequences satisfying $\alpha = [\alpha', t_w]$ are classified into the *trajectory class* represented by $\{H_n^\alpha\}$. The H_n^α 's sharing the same α' in α indicates that these trajectories originate from the same mother trajectory but under the action of a quantum jump at different time t_w . Assuming that the memory time is infinitely long, the trajectories belong to the $\{H_n^\alpha\}$ will be brought back to the same quantum state by the reversed quantum jump.

The K_n^α , referred to as the *existence probability*, represents the weight of the realizations staying in the state $|\psi_n^\alpha(t_s)\rangle$ in the limit of infinite number of realizations. Apparently, the sum of all the existence probability should be one by definition. The details in deriving the explicit expression of K_n^α can be found in Ref. [45] and we apply the result to the present model.

Since the jump operator in Eq. (8) is unitary, i.e. $(\sigma_A^x)^2 = \mathbb{I}$, the probability of a normal quantum jump in the regime of positive $\gamma_0(t)$ is given by $p_n^\alpha(t) = \gamma_0(t)\delta t$ which is state-independent. Therefore the existence probability of the no-jump trajectory yields

$$K_0^\alpha(t_w) = \prod_{s=1}^{w-1} [1 - \gamma_0(t_s)\delta t]. \quad (21)$$

By virtue of Eq. (21), the existence probability K_n^α of a generic trajectory with $n \geq 1$ at the end of the $\gamma_0 > 0$ period, i.e. the moment $t = t_P$, can be obtained iteratively as follows,

$$K_n^\alpha(t_P) = K_{n-1}^{\alpha'}(t_{w-1})\gamma_0(t_w)\delta t \prod_{s=w+1}^P [1 - \gamma_0(t_s)\delta t]. \quad (22)$$

The survival of H_n^α at t_P is a consequence of quantum trajectory $H_{n-1}^{\alpha'}$ undergoes a quantum jump at time t_w followed by no more jumps until t_P .

In the period of $\gamma_0 < 0$, the normal quantum jump is suspended while the *reversed* quantum jump is switched on. The former prohibits the creation of new quantum trajectory and the latter allows the existing quantum trajectory to jump back to its mother trajectory. The existence probability of K_0^α shares the same form as Eq. (21) for $\gamma_0 < 0$, therefore the coherence is restored as K_0^α increases. For a generic trajectory, after the first time interval of the $\gamma(t) < 0$ period, the existence probability of H_n^α is given as follows,

$$K_n^\alpha(t_P + \delta t) = K_n^\alpha(t_P) \left[1 - \gamma_0(t_P)\delta t \left(1 - \frac{K_{n-1}^{\alpha''}(t_P)}{\sum_\alpha K_n^\alpha(t_P)} \right) \right]. \quad (23)$$

The second term represents the increasing of K_n^α due to the reversed jump from the subclass of H_n^α while the third term represents the decreasing of K_n^α due to the reversed jump from K_n^α to its mother trajectory.

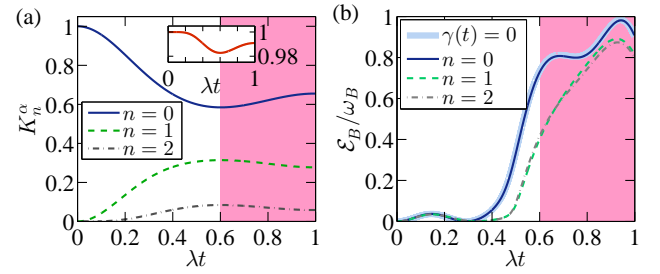


FIG. 4: (a) The existence probabilities of the no-jump, one-jump and two-jump trajectory classes. During the period of positive decay rate the K_0^α decreases due to the actions of the normal jumps while the H_1^α and H_2^α trajectories are created. The inset shows the sum of the existence probabilities up to $n = 2$ which is close to one throughout the time window. (b) The thick line represents the ergotropy under unitary time evolution. The solid, dashed and dash-dotted (thin) lines represent the ergotropy with respect to the density matrix computed by the NMQJ method with the summation up to $n = 0, 1$, and 2, respectively. The initial state is $|\uparrow_A^y \downarrow_B^z\rangle$. The coupling between the charger and the battery is $g = 4$ and the time interval is $\delta t = 5 \times 10^{-4} \lambda^{-1}$. Other parameters are chosen the same as in Fig. 3.

In Fig. 4(a) it is shown the time-evolution of the existence probabilities with various n . In the $\gamma_0 > 0$ period, the K_0^α decreases while K_1^α and K_2^α increase as the normal jumps take place. In contrast, in the $\gamma_0 < 0$ period, a revival of K_0^α can be observed due to the contribution from the K_1^α and K_2^α . Moreover, as shown in the inset of Fig. 4(a), the sum $\sum_{n=0}^2 K_n^\alpha$ also exhibits a revival in the $\gamma_0 < 0$ period and the magnitude is larger than 0.98 throughout the time window. Therefore, for the decay rate presented in Fig. 2(a), the sum in Eq. (18) can be truncated at $n = 2$ to construct the density matrix.

In order to reveal the contribution of each trajectory class in constructing the density matrix, we compare the ergotropies of the quantum battery with respect to the pure state under unitary time evolution [case(iii), $\gamma_0 = 0$] and to the state of the no-jump trajectory [case(i) with the sum in Eq. (18) truncated at $n = 0$]. As shown by the thick and thin solid lines in Fig. 4(b), these two results coincide. This is because the identity matrix in the imaginary part of \hat{H}_{eff} only introduces a global coefficient to $|\psi_0^\alpha\rangle$ which is proportional to γ_0 . The impact of the dephasing manifests in trajectories that have undergone at least one quantum jump. The ergotropy computed by the density matrix with the summation up to 1 and 2 are shown by the dashed and dash-dotted lines in Fig. 4(b). One can see that the ergotropy converges at $n = 2$ indicating the contributions from the quantum trajectories that undergo more than two quantum jump can be neglected. Moreover, for $0.4 \lesssim \lambda t \lesssim 0.6$ the ergotropy in the dephased time evolution deviates from that in the unitary evolution due to the creation of the trajectories belong to H_n^α and H_2^α . When entering into the region of $\gamma_0 < 0$, the reversed quantum jump brings the H_n^α and H_2^α trajectories back to the no-jump trajectory. Therefore the ergotropy under dephasing evolution becomes closer to that under unitary evolution because the history of dephasing being (partly) cancelled. At this sense, the negative γ_0 can be considered as a

signal of the memory effect.

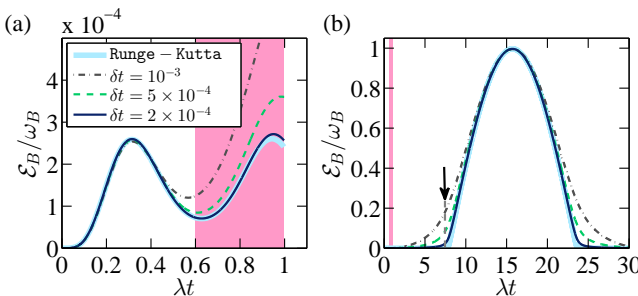


FIG. 5: (a) The early-stage time evolution of the ergotropy. The thick solid line represents the results computed by the forth-order Runge-Kutta method, while the thin solid, dashed, and dot-dashed line represent the NMQJ results with time interval $\delta t = 2 \times 10^{-4} \lambda^{-1}$, $5 \times 10^{-4} \lambda^{-1}$ and $10^{-3} \lambda^{-1}$, respectively. (b) The long-time evolution of the ergotropy. The coupling strength between the charger and the battery is chosen as $g = 0.2$ and other parameters are chosen the same as in Fig. 3.

V. MEASUREMENT-ENHANCED QUANTUM BATTERY

The implementation of the NMQJ method assumes that time interval δt is so short that only one quantum jump takes place during δt . To verify, the comparison of the ergotropies computed by the forth-order RK method and by the NMQJ method with various δt is shown in Fig. 5(a). To highlight the effects of the non-Markovianity, the case of weak coupling between the charger and the battery is considered in which the early-stage behavior is mainly governed by the dephasing.

One can see that the NMQJ result agrees with the RK result when the time interval is chosen as $\delta t = 2 \times 10^{-4} \lambda^{-1}$. A large δt causes the state of the quantum battery to deviate from the true one at the end of the $\gamma < 0$ region. Although the results obtained with larger δt are incorrect concerning the solution to Eq. (17), it is still worthy to investigate the subsequent dynamics and, as be illustrated below, may motivate a scenario to enhance the performance of quantum battery.

We take the temporal states at the end of the $\gamma_0 < 0$ region to continue the time evolution in the subsequent $\gamma_0 > 0$ region. The long-time behaviors are shown in Fig. 5(b). One can see that the time evolution of the ergotropy with a history of larger δt exhibit an significant advantage over the others. In more detail, as indicated by the vertical arrow, the quantum battery which allows only one quantum jump within $\delta t = 10^{-3} \lambda^{-1}$ in the early stage has been charged to 20 percents ergotropy at $\lambda t \approx 7.5$, whereas the ergotropy of the battery under other conditions remains far below.

Recall that in the NMQJ implementation, the physical meaning of δt is the time window over which the system either evolves continuously or undergoes an action of local coherent flip on the charger. The probability is essentially determined by the time-dependent γ_0 . In the limit of $\delta t \rightarrow 0$, the NMQJ method precisely simulate the dynamics described by the mas-

ter equation (8). This motivates us to design a quantum circuit acting the CmB system as shown in Fig. 1(b). It is composed of the global unitary operation \hat{U}_{AB} and the probabilistic local coherent spin flip operation $\hat{\sigma}_A^x$. The global operation is generated by the Hamiltonian $\hat{H}_0 + \hat{H}_1$ over an evolution time δt , i.e. $\hat{U} = \exp[-i(\hat{H}_0 + \hat{H}_1)\delta t]$. The probability whether to implement the local $\hat{\sigma}_A^x$ or not is determined by $\gamma_0(t)\delta$. This circuit provides a physical realization for curve of ergotropy in Fig. 5 and thus enables to enhance the performance of the quantum battery.

VI. SUMMARY

In summary, we have demonstrated the early-stage memory effect on the performance of the dephasing CmB system consisted of two qubits. From a microscopic derivation, we obtained the time-local master equation in Lindblad form with local dephasing on the charger qubit. The time-dependent dephasing rate $\gamma_0(t)$ exhibit an oscillation at the early time and then approaches to the asymptotic value $\gamma_0(\infty)$ in the late time. The temporal negative γ_0 violates the complete positivity of the master equation and leading to a non-Markovianity of the dynamics of the CmB system. We found that the strong non-Markovianity is beneficial to the performance of the quantum battery. In comparison with the Markovian CmB system with the constant dephasing rate $\gamma_0(\infty)$, the non-Markovian one increases the maximal ergotropy at the end of the charging process. This is because the memory effect during the $\gamma_0 < 0$ region tends to recover the performance of the battery under unitary evolution.

In order to highlight the memory effect, we adopted the NMQJ method to unravel the Lindblad master equation. We found that the time evolution of the ergotropy with respect to the no-jump state exhibits the same behavior as that in the unitary evolution. The deviation of the ergotropy in the dephased scenario is due to the contributions from the trajectory classes with at least one quantum jump. Actually, we show that a truncation at $n = 2$ is sufficient for the sum to construct the density matrix. The reversed jump in the period of $\gamma_0 < 0$ period transforms the H_1^α and H_2^α trajectories to the no-jump trajectory level by level. Therefor the information lost in earlier time is recovered and the maximal ergotropy could exceed the one in the process under Markovian approximation.

The time interval is essential in the simulation by the NMQJ method. We show that a larger time interval may lead the numerical result to deviate from the true value. Because the number of quantum jumps are restricted so that the continuous time evolution cannot be effectively simulated. Moreover the deviations remain in the subsequent time-evolution and is responsible for an enhancement of the battery performance. This motivates us to propose a discrete time measurement-enhanced scheme at the early-stage of the charging process. A quantum circuit version of such a scheme is proposed. With a relatively larger time interval, the state at the end of the non-Markovian region may lead to an improvement of the charging speed.

ACKNOWLEDGMENTS

J.J. thanks Prof. H. Z. Shen for valuable discussion. This work is supported by Natural Science Foundation of Liaoning Province of China No. 2025-MS-009.

Appendix A: Microscopic derivation of the master equation

In the Scrödinger picture, the Hamiltonian of the full Hamiltonian of the CmB system is given as follows,

$$\begin{aligned}\hat{H} &= \hat{H}_A + \hat{H}_B + \hat{H}_E + \hat{H}_A^{\text{dr}} + \hat{H}_{AB} + \hat{H}_{AE} \\ &= \hat{H}_{\bar{A}} + \hat{H}_B + \hat{H}_{AB} + \hat{H}_{AE}\end{aligned}\quad (\text{A1})$$

where the terms are presented in Eqs. (1)-(6) of the main text. We have combined the \hat{H}_A and \hat{H}_A^{dr} as the local Hamiltonian of the charger $\hat{H}_{\bar{A}}$.

In the rotating frame of $\frac{\omega_L}{2}\hat{\sigma}_A^z$, the interaction Hamiltonians yield

$$\hat{H}_{AB} = g e^{i\omega_L t} \hat{\sigma}_A^+ \hat{\sigma}_B^- + \text{h.c.}, \quad (\text{A2})$$

and

$$\hat{H}_{AE} = \sum_k (g_k e^{i\omega_L t} \hat{\sigma}_A^+ \hat{a}_k + \text{h.c.}). \quad (\text{A3})$$

The local Hamiltonian of the charger $\hat{H}_{\bar{A}}$ yields

$$\hat{H}_{\bar{A}} = \frac{\Delta}{2} \hat{\sigma}_A^z + \frac{\Omega}{2} \hat{\sigma}_A^x = \frac{\omega}{2} \hat{\sigma}_A^z, \quad (\text{A4})$$

where where $\Delta = \omega_A - \omega_L$. The free Hamiltonians \hat{H}_B and \hat{H}_E remains invariant.

The eigenvalues of the local Hamiltonian of the charger can be obtained as $\pm \frac{\omega}{2}$ where $\omega = \sqrt{\Delta^2 + \Omega^2}$. The eigenbasis are

$$|+_A\rangle = \cos \frac{\theta}{2} | \uparrow_A^z \rangle + \sin \frac{\theta}{2} | \downarrow_A^z \rangle, \quad (\text{A5})$$

and

$$|-_A\rangle = \sin \frac{\theta}{2} | \uparrow_A^z \rangle - \cos \frac{\theta}{2} | \downarrow_A^z \rangle. \quad (\text{A6})$$

In representation of the eigenbasis $\{|+_A\rangle, |-_A\rangle\}$, the operators of the charger A becomes

$$\hat{H}_{\bar{A}} = \frac{\omega}{2} \hat{\sigma}_A^z, \quad (\text{A7})$$

and

$$\hat{\sigma}_A^+ = \frac{1}{2} (\sin \theta \hat{\sigma}_A^z - \cos \theta \hat{\sigma}_A^x - i \hat{\sigma}_A^y), \quad (\text{A8})$$

the Pauli operator with a bar means that it lives in the representation of the eigenbasis of A .

Define $\hat{U}_0 = \exp[-i(\hat{H}_{\bar{A}} + \hat{H}_B + \hat{H}_E)t]$ and $\hat{U} = \exp(-i\hat{H}t)$. In the weak-coupling limit between the charger and the reservoir, one can use the time-convolutionless projection operator technique and obtain the Liouville equation in the interaction picture as follows,

$$\begin{aligned}\dot{\rho}_I(t) &= -i[\bar{H}, \rho_I(t)] \\ &= -i[\bar{H}_{AB,I}, \rho(t)] \\ &\quad - \int_0^t [\bar{H}_{AE,I}, [\bar{H}_{AE,I}(s), \rho_I(t)]] ds.\end{aligned}\quad (\text{A9})$$

The master equation for the CmB system can be derived by tracing over E of Eq. (A9). In the limit of a continuum of the reservoir modes $\sum_k g_k^2 \rightarrow \int J(\omega) d\omega$ with the spectral density $J(\omega)$. Assume the spectral density is the Lorentzian as shown in Eq. (7) and back to the Schrödinger picture, the master equation can be obtained as

$$\dot{\rho}_{AB} = -i[\bar{H} + \hat{H}_B + \hat{H}_{AB}, \rho_{AB}(t)] + \mathcal{D}_A[\rho_{AB}(t)], \quad (\text{A10})$$

where the local dissipator \mathcal{D}_A can be divided into the secular part \mathcal{D} and the nonsecular part [29]. The nonsecular part vanishes when the parameter $p \gg 1$. The secular part is given by

$$\begin{aligned}\mathcal{D}[\rho_{AB}] &= \gamma_+(t)[\bar{\sigma}_A^- \rho_{AB}(t) \bar{\sigma}_A^+ - \frac{1}{2}\{\bar{\sigma}_A^+ \bar{\sigma}_A^-, \rho_{AB}(t)\}] \\ &\quad + \gamma_-(t)[\bar{\sigma}_A^+ \rho_{AB}(t) \bar{\sigma}_A^- - \frac{1}{2}\{\bar{\sigma}_A^- \bar{\sigma}_A^+, \rho_{AB}(t)\}] \\ &\quad + \gamma_0(t)[\bar{\sigma}_A^z \rho_{AB}(t) \bar{\sigma}_A^z - \rho_{AB}(t)].\end{aligned}\quad (\text{A11})$$

For the reservoir with a Lorentzian spectral density, the explicit expression of the time-dependent decay rates are obtained in Ref. [28]. We borrow the result and show it in below

$$\gamma_\xi(t) = \frac{\eta^2 C_\xi}{2(1+q_\xi^2)} (1 - e^{-\lambda t} \cos(q_\xi \lambda t) + e^{-\lambda t} q_\xi \sin(q_\xi \lambda t)), \quad (\text{A12})$$

where $q_\xi = s - \xi p$ with $\xi = \{+, -, 0\}$. The behavior of the decay rate for $p = 100$ and $s = 6$ is shown in Fig. 2(a) of the main text. One can see that the amplitude of γ_\pm is so small compared with γ_0 that can be neglected.

For the resonant case $\Delta = 0$, the eigenbasis is specialized to $|+_A\rangle = | \uparrow_A^x \rangle$ and $|-_A\rangle = | \downarrow_A^x \rangle$ and the coefficient are given by $C_+ = C_0 = \frac{1}{2}$ and $C_- = -\frac{1}{2}$. The local Hamiltonian in the σ^z -representation can be expressed as $\hat{H}_{\bar{A}} = -\frac{\Omega}{2} \hat{\sigma}_A^x$. Therefore, the dissipator in Eq. (A11) reduces to Eq. (11) in the main text.

[1] R. Horodecki, P. Horodecki, M. Horodecki, and K. Horodecki, Quantum entanglement, Rev. Mod. Phys. **81**, 865 (2009).

[2] F. Campaioli, S. Gherardini, J. Q. Quach, M. Polini, and G. M.

Andolina, *Colloquium: Quantum batteries*, Rev. Mod. Phys. **96**, 031001 (2024).

[3] F. C. Binder, S. Vinjanampathy, K. Modi, and J. Goold, Quantum-cell: powerful charging of quantum batteries, New J. Phys. **17**, 075015 (2015).

[4] D. Ferraro, M. Campisi, G. M. Andolina, V. Pellegrini, and M. Polini, High-Power Collective Charging of a Solid-State Quantum Battery, Phys. Rev. Lett. **120**, 117702 (2018).

[5] F. Barra, Dissipative charging of a Quantum Battery, Phys. Rev. Lett. **122**, 210601 (2019).

[6] S. Seah, M. Perarnau-Llobet, G. Haack, N. Brunner, and S. Nimmrichter, Phys. Rev. Lett. **127**, 100601 (2021).

[7] D. Rossini, G. M. Andolina, D. Rosa, M. Carrega, and M. Polini, Quantum Advantage in the Charging Process of Sachdev-Ye-Kitaev Batteries, Phys. Rev. Lett. **125**, 236402 (2020).

[8] G. Francica, F. C. Binder, G. Guarneri, M. T. Mitchison, J. Goold, and F. Plastina, Quantum coherence and ergotropy, Phys. Rev. Lett. **125**, 180603 (2020).

[9] P. Chen, T. S. Yin, Z. Q. Jiang, and G. R. Jin, Quantum enhancement of a single quantum battery by repeated interactions with large spins, Phys. Rev. E **106**, 054119 (2022).

[10] F. Q. Dou, Y. Q. Lu, Y. J. Wang, and J. A. Sun, Extended Dicke quantum battery with interatomic interactions and driving field, Phys. Rev. B **105**, 115405 (2022).

[11] F. Q. Dou, H. Zhou, and J. A. Sun, Cavity Heisenberg-spin-chain quantum battery, Phys. Rev. A **106**, 032212 (2022).

[12] M. L. Song, L. J. Li, X. K. Song, L. Ye, and D. Wang, Environment-mediated entropic uncertainty in charging quantum batteries, Phys. Rev. E **106**, 054107 (2022).

[13] J. S. Yan and J. Jing, Charging by quantum measurement, Phys. Rev. Appl. **19**, 064069 (2023).

[14] W.-L. Wang, H.-B. Liu, B. Zhou, W.-L. Yang, and J.-H. An, Remote Charging and Degradation Suppression for the Quantum Battery, Phys. Rev. Lett. **132**, 090401 (2024).

[15] S.-Q. Liu, L. Wang, H. Fan, F.-L. Wu, and S.-Y. Liu, Better performance of quantum batteries in different environments compared to closed batteries, Phys. Rev. A **109**, 042411 (2024).

[16] T. Zhang, H. Yang, and S.-M. Fei, Local-projective-measurement-enhanced quantum battery capacity, Phys. Rev. A **109**, 042424 (2024).

[17] W.-L. Wang, J.-L. Wang, B. Zhou, W.-L. Yang, and J.-H. An, Self-Discharging Mitigated Quantum Battery, Phys. Rev. Lett. **135**, 020405 (2025).

[18] R. Shastri, C. Jiang, G.-H. Xu, B. P. Venkatesh, and G. Watanabe, Dephasing enabled fast charging of quantum batteries, npj Quantum Inf. **11**, 9 (2025).

[19] A. Canzio, V. Cavina, M. Polini, V. Giovannetti, Single-atom dissipation and dephasing in Dicke and Tavis-Cummings quantum batteries, Phys. Rev. A **111**, 022222 (2025).

[20] Y. Yao and X. Q. Shao, Reservoir-assisted quantum battery charging at finite temperatures, Phys. Rev. A **111**, 062616 (2025).

[21] M.-L. Hu, T. Gao and H. Fan, Efficient wireless charging of a quantum battery, Phys. Rev. A **111**, 042216 (2025).

[22] H.-P. Breuer and F. Petruccione, *The Theory of Open Quantum Systems* (Oxford University Press, New York, 2002).

[23] D. Farina, G. M. Andolina, A. Mari, M. Polini, V. Giovannetti, Charger-mediated energy transfer for quantum batteries: An open-system approach, Phys. Rev. B **99**, 035421 (2019).

[24] H.-P. Breuer, E.-M. Laine, and J. Piilo, Measure for the degree of non-Markovian behavior of quantum processes in open systems, Phys. Rev. Lett. **103**, 210401 (2009).

[25] Á. Rivas, S. F. Huelga, and M. B. Plenio, Entanglement and non-Marokivianity of Quantum Evolutions, Phys. Rev. Lett. **105**, 050403 (2010).

[26] J. L. Li, H. Z. Shen, and X. X. Yi, Quantum batteries in non-Markovian reservoirs, Opt. Lett. **47**, 5614 (2022).

[27] D. Morrone, M. A. C. Rossi, A. Smirne, and M. G. Genoni, Charging a quantum battery in a non-Markovian environment: a collisional model approach, Quantum Sci. Technol. **8**, 035007 (2023).

[28] P. Haikka and S. Maniscalco, Non-Markovian dynamics of a damped driven two-state system, Phys. Rev. A **81**, 052103 (2010).

[29] P. Haikka, Non-Markovian master equation for a damped driven two-state system, Phys. Scr. **T140**, 014047 (2010).

[30] G. Lindblad, On the generators of quantum dynamical semigroups, Commun. Math. Phys. **48**, 119 (1976).

[31] V. Gorini, A. Kossakowski, and E. C. G. Sudarshan, Completely positive dynamical semigroups of N-level systems, J. Math. Phys. **17**, 821 (1976).

[32] J. Dalibard, Y. Castin, and K. Mølmer, Wave-function approach to dissipative processes in quantum optics, Phys. Rev. Lett. **68**, 580 (1992).

[33] K. Mølmer, Y. Castin, and J. Dalibard, Monte Carlo wavefunction method in quantum optics, J. Opt. Soc. Am. B **10**, 524 (1993).

[34] M. B. Plenio and P. L. Knight, The quantum-jump approach to dissipative dynamics in quantum optics, Rev. Mod. Phys. **70**, 101 (1998).

[35] A. J. Daley, Quantum trajectories and open many-body quantum systems, Adv. Phys. **63**, 77 (2014).

[36] J. Piilo, S. Maniscalco, K. Härkönen, and K.-A. Suominen, Non-Markovian Quantum Jumps, Phys. Rev. Lett. **100**, 180402 (2008).

[37] J. Piilo, K. Härkönen, S. Maniscalco, and K.-A. Suominen, Open system dynamics with non-markovian quantum jumps, Phys. Rev. A **79**, 062112 (2009).

[38] A. Smirne, M. Caiaffa, and J. Piilo, Rate Operator Unraveling for Open Quantum System Dynamics, Phys. Rev. Lett. **124**, 190402 (2020).

[39] K. Luoma, W. T. Strunz, and J. Piilo, Diffusive Limit of Non-Markovian Quantum Jumps, Phys. Rev. Lett. **125**, 150403 (2020).

[40] D. Chruściński, K. Luoma, J. Piilo, and A. Smirne, How to design quantum-jump trajectories via distinct master equation representations, Quantum **6**, 835 (2022).

[41] B. Donvil and P. Muratore-Ginanneschi, Quantum trajectory framework for general time-local master equations, Nat. Commun. **13**, 4140 (2022).

[42] T. Becker, C. Netzer, and A. Eckardt, Quantum Trajectories for Time-Local Non-Lindblad Master Equations, Phys. Rev. Lett. **131**, 160401 (2023).

[43] F. Settimi, K. Luoma, D. Chruściński, B. Vacchini, A. Smirne and J. Piilo, Generalized-rate-operator quantum jumps via realization-dependent transformations, Phys. Rev. A **109**, 062201 (2024).

[44] G. Chiriacò, M. Tsitsishvili, D. Poletti, R. Fazio, and M. Dalmonte, Diagrammatic method for many-body non-Markovian dynamics: Memory effects and entanglement transitions, Phys. Rev. B **108**, 075151 (2023).

[45] H. Zhang and J. Jin, Non-Markovian quantum jump method for driven-dissipative two-level systems, Phys. Rev. A **112**, 062214 (2025).

[46] W. K. Wootters, Entanglement of formation of an arbitrary state of two qubits, Phys. Rev. Lett. **80**, 2245 (1998).

[47] A. E. Allahverdyan, R. Balian, and T. M. Nieuwenhuizen, Max-

imal work extraction from finite quantum system, *Europhys. Lett.* **67**, 565 (2004).

[48] H. L. Shi, S. Ding, Q. K. Wan, X. H. Wang, and W. L. Yang, Entanglement, coherence, and extractable work in quantum batteries, *Phys. Rev. Lett.* **129**, 130602 (2022).